The Hertz/VPM polarimeter: design and first light observations

Megan Krejny,[1,*] David Chuss,[2] Christian Drouet d'Aubigny,[3] Dathon Golish,[3] Martin Houde,[4] Howard Hui,[2,5] Craig Kulesa,[3] Robert F. Loewenstein,[6] S. Harvey Moseley,[2] Giles Novak,[1] George Voellmer,[2] Chris Walker,[3] and Ed Wollack[2]

[1]Northwestern University, Department of Physics and Astronomy, 2131 Tech Drive, Evanston, Illinois 60208, USA

[2]NASA Goddard Space Flight Center, Greenbelt, Maryland 20771, USA

[3]University of Arizona, Steward Observatory, 933 North Cherry Avenue, Tucson, Arizona 85721, USA

[4]The University of Western Ontario, Department of Physics and Astronomy, London, Ontario N6A 3K7, Canada

[5]Oregon State University, Department of Physics, 301 Weniger Hall, Corvallis, Oregon 97331, USA

[6]University of Chicago, Yerkes Observatory, 373 West Geneva Street, Williams Bay, Wisconsin 53191, USA

*Corresponding author: m-krejny@northwestern.edu

Received 26 March 2008; revised 17 July 2008; accepted 17 July 2008; posted 18 July 2008 (Doc. ID 94294); published 19 August 2008

We present first results of Hertz/VPM, the first submillimeter polarimeter employing the dual Variable-delay Polarization Modulator (dual-VPM). This device differs from previously used polarization modulators in that it operates in translation, rather than mechanical rotation. We discuss the basic theory behind this device and its potential advantages over the commonly used half-wave plate. The dual-VPM was tested both at the Submillimeter Telescope Observatory and in the laboratory. In each case we present a detailed description of the setup. We discovered that properties of the VPM wire grids (diameter and spacing) caused behavior that differs from theoretical predictions for ideal wire grid performance. By modifying the polarimeter settings to compensate for this behavior, we found that the dual-VPM system is robust, operating with high efficiency and low instrumental polarization. This device is well suited for air- and space-borne applications.

OCIS codes: 350.1260, 120.5410.

1. Introduction

It has been almost 60 years since the discovery of the polarization of starlight by magnetically aligned dust grains [1–3]. Since then, astronomical polarimetry has become a valuable and well-established tool to study a wide variety of astrophysical sources, from nearby star-forming regions to the radiation linked to the formation of our universe. Polarized submillimeter and far infrared (FIR) light from thermally emitting aligned dust grains, both in the interstellar medium and around stars, allows us to map the plane-of-sky magnetic field in these regions [4–6]. In star-forming regions, light along the line of sight is emitted by dust grains at different temperatures; to separate cooler dust contributions from the warmer dust, e.g., near protostars, observations at multiple wavelengths are required. Astronomical polarimetry is also of great interest in cosmology. Measuring the polarization of the cosmic microwave background (CMB) could provide an opportunity to study the universe during its first $\sim 10^{-32}$ s after the Big Bang, when the universe is thought to have gone through an

0003-6935/08/244429-12$15.00/0

inflationary epoch at an energy scale ~12 orders of magnitude above those accessible to terrestrial particle accelerators.

Whether observing star-forming regions or remnants of the early universe, one faces the same primary challenge: measuring polarized fluxes that are 10^{-6} or less of the total incident flux. For dust and gas clouds, polarizations are often on the order of 10^{-2} of the total source flux, but very small (10^{-6}) compared to the atmospheric flux (for ground-based observations). For the CMB, the polarized flux is a million times below the total CMB power. The polarized signature from inflationary physics is expected to be even lower (10^{-7} to 10^{-9}) [7].

Measuring a small polarized signal in the presence of a large, unpolarized background is challenging. Noise from the background as well as time variations in the instrument and observing environment dominate the signal. Polarization modulation allows for encoding the polarization signal, enabling a subsequent extraction of the signal from the more random data stream.

In this paper, we describe the implementation of a novel polarization modulator, the dual Variable-delay Polarization Modulator, or dual-VPM. The dual-VPM operates in reflection instead of transmission, and fully modulates the linear polarization state using only small translational motions. These properties make the dual-VPM an attractive alternative to the conventional birefringent half-wave plate (HWP) modulator for certain applications. We review the basic principle of the dual-VPM and describe the development and characterization of this device.

We used Hertz, a polarimeter previously used at the Caltech Submillimeter Observatory (CSO), as a dual-polarization detector for our dual-VPM system. This new Hertz/VPM polarimeter was tested at 350 μm at the Submillimeter Telescope Observatory (SMTO), where we characterized the performance of the VPMs. Follow-up data were later collected at Northwestern University. We present the results from these two tests. We find that the dual-VPM system is robust, operating with high efficiency and low instrumental polarization.

2. Polarimetric Techniques

A. Stokes Parameters

Full characterization of electromagnetic radiation requires knowledge of its amplitude and phase. For partially coherent radiation fields, this information is encoded in the time-averaged correlations between orthogonal fields. These are well parameterized by the *Stokes parameters*, which describe the total flux (I), linearly polarized flux (Q and U), and circularly polarized flux (V) [8]. These four quantities are related by

$$I^2 \geq Q^2 + U^2 + V^2, \tag{1}$$

where equality holds for fully polarized light. Following the convention of [8], we denote (for light propagating toward the viewer) Stokes Q to be the difference between horizontal and vertical polarization, and Stokes U as the difference between linear polarization oriented +45° and −45°. The angle of polarization is defined to increase counterclockwise from the horizontal. Normalized Stokes parameters (Q/I, U/I, V/I) are denoted by q, u, and v.

B. The Half-Wave Plate and the Variable-delay Polarization Modulator

The HWP is a device that is able to induce a half-wave phase delay between incident orthogonal polarization components. For this paper (unless otherwise specified) we will use the term "HWP" to mean a birefringent device (for example, a quartz crystal) cut such that its optic axis is parallel to the front and back surfaces (orthogonal to the direction of light propagation) and whose thickness is chosen such that the plate will induce a 180° phase delay between orthogonal polarization components. A rotation of the HWP by an angle θ causes a rotation of the plane of polarization by a corresponding 2θ. The HWP can be summarized as a device that induces a fixed delay between orthogonal components, in effect rotating the polarization basis.

A "reflective HWP" can be constructed by rotating a polarizing grid in front of a mirror. Light incident upon the grid is separated into polarization either parallel or perpendicular to the grid wires. The former is reflected by the grid while the latter is transmitted to the mirror, reflects, and then recombines with the orthogonal counterpart (Fig. 1). For light with an incident angle of θ_{inc}, the induced path-length difference l is given by

$$l = 2d \cos \theta_{\mathrm{inc}}. \tag{2}$$

If we set this path-length difference to $\lambda/2$, the device functions as a HWP in reflection. Rotation of the grid is physically equivalent to rotating a HWP. This

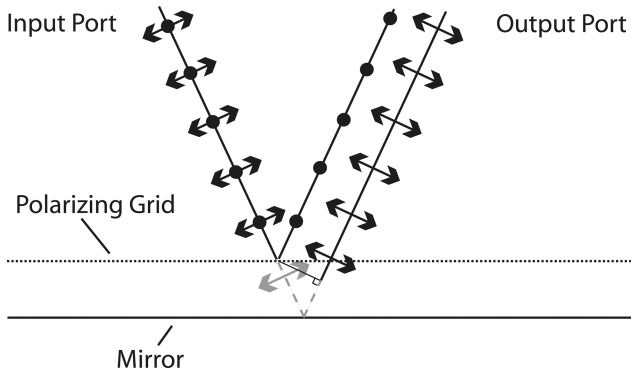

Fig. 1. "Reflective half-wave plate." Light incident upon a wire grid is separated into orthogonal polarization components; the component parallel to the wire grid is reflected while the perpendicular component is transmitted and reflected by a mirror, traveling an extra distance l (dashed line). When the delay l is set equal to half of the wavelength, this device has the same functionality as a birefringent half-wave plate (HWP).

type of device has been used for astronomical polarimetry at millimeter wavelengths [9,10].

Suppose that, instead of maintaining a fixed distance between the grid and mirror surfaces, we now move the mirror back and forth, thus changing the physical path-length difference between the orthogonal polarization components. By doing so, we fix the polarization basis and vary the phase delay; devices of this type have been denoted Variable-delay Polarization Modulators, or VPMs [11].

One VPM switched between half- and full-wave delays is equivalent to turning a HWP "on" or "off," that is, moving a HWP in and out of the beam. We can calculate the necessary grid–mirror separation distances from Eq. (2); for example, 350 μm light incident at 20° requires settings of 93 and 186 μm separations, respectively. However, if polarization incident on the VPM grids is either completely parallel or perpendicular to the grid, then the polarization will not be modulated, regardless of the separation distance.

This problem can be solved by placing two VPMs in series with their grids rotated by 22.5° with respect to one another (corresponding to 45° in Stokes space); see Fig. 2. In this way, any polarization not modulated by one VPM will be modulated by the other. We also set the grid angle of the second VPM to be rotated 45° with respect to the analyzer grid used for the detector. This dual-VPM system will accurately reproduce the function of a rotating HWP [11].

Single VPMs have been used for astronomical polarimetry at millimeter wavelengths in the form of a modified Martin–Puplett Interferometer [12]. However, since only one VPM was used, another modulator (double-Fresnel rhomb) had to be incorporated. The dual-VPM modulation scheme has the advantage of requiring only small translational motions, rather than rotation, to obtain full modulation of all linear polarization states. This paper reports the first astronomical observations using a submillimeter polarimeter incorporating a dual-VPM system.

The VPM has several advantages over the HWP. The VPM, in contrast to the birefringent HWP, operates in reflection and, so, avoids some of the drawbacks of dielectrics. Also, assuming near-perfect grid performance over a large range of wavelengths, the wavelength of operation for the VPM can be easily tuned. In comparison, for multiwavelength operation the dielectric HWP requires multiple birefringent layers and complicated (and often costly) achromatic antireflective coatings. The VPM operates without a rotation bearing; the small motion of the mirror can be accomplished via piezoelectric motors and flexure bearings. Flexure bearings operate without friction and are generally considered to be the most durable of all nonlevitating bearings. Finally, the freedom of a variable delay means that the VPM can also act as a quarter-wave plate. For broadband continuum work, the magnitude of astronomical circular polarization is often expected to be negligible; thus, measuring circular polarization can allow a check of the systematics of an experiment.

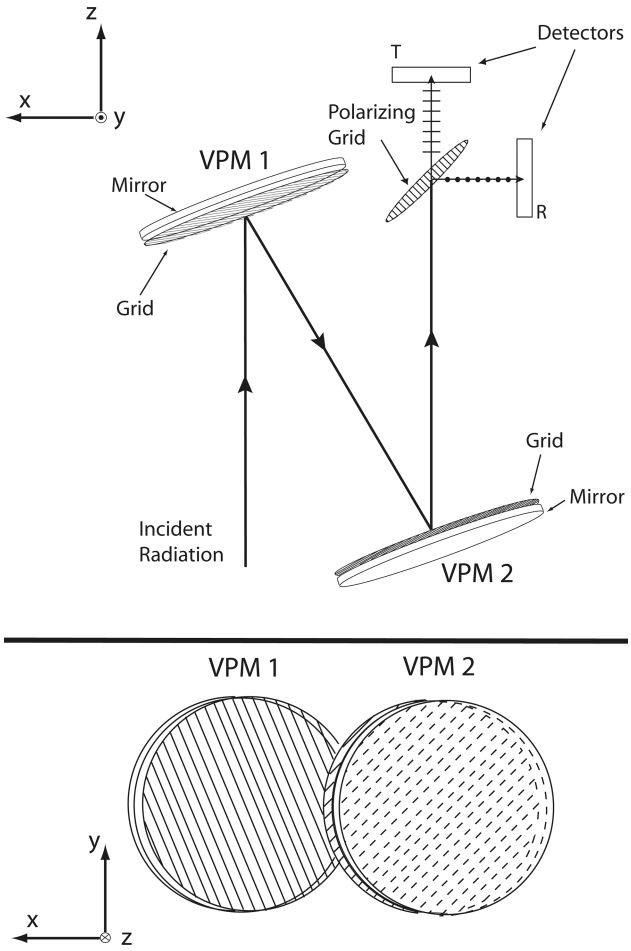

Fig. 2. Two views of a schematic optical path for a polarimeter incorporating a dual-VPM modulator. The upper panel shows a top view while the lower panel shows the view "seen" by the incoming radiation. The radiation is reflected by two VPMs having their grid wires rotated by 22.5° with respect to one another and is then incident upon a polarizing grid that splits the beam into orthogonal polarization components directed to detectors R and T (standing for reflected and transmitted). Note that the figure is a general schematic and is not representative of the actual grid settings and orientations used for the Hertz/VPM experiment.

The VPM does have challenges in its construction, characterization, and operation. The desire for high tolerances (we chose general tolerances below 10 μm) requires careful design. It also makes the device susceptible to large systematic vibrations. Also, error caused by nonparallel grid and mirror surfaces must be carefully minimized, requiring longer setup times than for the HWP. High grid efficiencies require flat and finely spaced wire grids, which can be expensive to produce. Finally, as we shall see in Subsection 4.A, VPM characterization is nontrivial. But first, we discuss basic polarization measurement techniques for the HWP and dual-VPM modulators.

C. Data Acquisition and Analysis

Now that we have discussed the operation of both the HWP and VPM, we wish to compare their use in

practical applications, i.e., for use with real submillimeter telescopes. We begin with a discussion of the methods used to derive polarization signals from a dual-polarization detector for a single modulator position. Below we start with a summary of basic data analysis techniques for submillimeter wavelengths from [13].

Removal of the proportionately large sky signal present in one's observations requires fast switching ("chopping") of the telescope beam between two points: the source itself and an off-source point. The chopping frequency must be fast enough to overcome $1/f$ noise from the atmosphere (often ranging from 3–15 Hz). As the secondary mirror is chopping between on and off source, data points are calculated by subtracting the voltage value of the "right" beam from that of the "left" beam.

One also "nods" the telescope, switching the source between the two beams. This nodding technique reduces effects caused by surface defects and temperature differentials across the primary mirror. We observe the object in a "left–right–right–left" ($l-r-r-l$) pattern in order to eliminate long-term linear progressions in the signal, for example, if the telescope mirror were slowly warming over time. Each nod in this "chop–nod" cycle contains an equal number of demodulated chop values; an average over all chops is saved for each nod: l_1, r_1, r_2, and l_2.

To observe dual polarization simultaneously, a polarizing grid is used to direct orthogonal linear polarization components into two detector arrays such that one array observes the reflected light and the other transmitted light. The intensity for one pixel in each array (reflected R or transmitted T) over one chop–nod cycle is calculated as

$$R(\text{or } T) = (l_1 - r_1 - r_2 + l_2)/4, \tag{3}$$

where the four terms refer to the averaged nod values as described above (r terms are subtracted, since they are negative values). The measured polarization signal S_{mod} for a given modulator position is

$$S_{\text{mod}} = \frac{(R_{\text{mod}} - fT_{\text{mod}})}{(R_{\text{mod}} + fT_{\text{mod}})}, \tag{4}$$

where f is the relative gain between the corresponding R and T pixels ($\sum R/\sum T$), averaged over all chop values for a full cycle. Stokes parameters are then calculated from the S_{mod} values for one modulator cycle in a manner determined by the type of polarization modulation used. We now present analysis techniques for both the HWP and dual-VPM systems.

We define one "HWP cycle" as a stepped rotation of the HWP through a set of angles spaced evenly over a 180° range. From Eq. (4), the polarization signal S_{mod} is plotted as a function of HWP angle θ ($S_{\text{mod}} \rightarrow S_\theta$) and a sine curve is fit to the data such that the amplitude of the curve gives the degree of polarization P and the phase of the curve gives the polarization angle φ. The fitting procedure is explained by [14]. It takes into account the arbitrary offset of the HWP zero angle relative to one's experiment. One must also adjust the sign of the HWP angle to account for the number of reflections between the HWP and the point of measurement.

For a "VPM cycle," the VPM grid–mirror separations are switched between "on" and "off" positions in four different combinations (VPM 1–VPM 2): pos1: on–on, pos2: on–off, pos3: off–on, and pos4: off–off. Here, "on" refers to a half-wave delay and "off" refers to a full-wave delay [11]. One calculates the Stokes parameters as follows [11]:

$$q = (S_{\text{pos2}} - S_{\text{pos1}})/2, \tag{5}$$

$$u = (S_{\text{pos4}} - S_{\text{pos3}})/2. \tag{6}$$

These equations are consistent with the convention that the time-reversed polarized light beams from the R and T detector arrays reach VPM 2 with polarization angles rotated by ±45° with respect to the grid wires of VPM 2 (e.g., see Fig. 2). This condition is necessary for full modulation of the polarization signal. Hertz/VPM is configured such that R is sensitive to Stokes $-U$ and T is sensitive to $+U$ (see Subsections 3.B and 3.C). If the arrays are role reversed in Eq. (4), one must set q to $-q$ and u to $-u$. P and φ then follow from Stokes definitions:

$$P = \sqrt{q^2 + u^2}, \tag{7}$$

$$\varphi = (1/2)\arctan(u/q). \tag{8}$$

The angle φ is thus defined relative to a coordinate system chosen by the observer. For Hertz/VPM we define φ relative to the coordinate system of our optics plane (Subsection 3.B); this angle can then be projected onto the sky.

These cycles were defined for a system with only one type of modulator installed. If both types are present, as we shall see is the case with our Hertz/VPM polarimeter, the above definitions are still applicable, provided one modulator is held fixed while the other is cycled.

3. Design of Hertz/VPM

Having described the theory behind the function of both the HWP and the dual-VPM polarimeters and their respective analysis techniques, we now describe the physical implementation of the Hertz/VPM polarimeter. The Hertz/VPM polarimeter consists of the dual-VPM modulator and the decomissioned CSO polarimeter, Hertz. An optics train, including the dual-VPM modulator, was built and used in front of Hertz. We tested the full Hertz/VPM system at SMTO on Mount Graham in Arizona from 16–24 April 2006. The following year, we conducted a series of

tests to further characterize Hertz/VPM in the laboratory at Northwestern University. Below we outline the construction of the VPMs and the experimental setup for both SMTO and the laboratory. This includes a description of the optics train as well as our use of the Hertz polarimeter.

A. VPM Construction

Our VPMs have four main elements: (1) an aluminum frame, consisting of a rectangular box with the top and back panels removed; (2) an optical quality mirror on a translation stage, mounted inside to the bottom of the frame; (3) a wire grid mounted to the front of the frame; and (4) a piezoelectric actuator, mounted in front of the frame that controls mirror motion [15].

The mirror is composed of vapor-deposited aluminum on glass and rests on a moving stage mounted on a kinematic variant of a double-blade flexure linear bearing. The main flexures are machined in an hourglass shape to improve the parallelism of the bearing during motion. This is shown in Fig. 3. The parallelism of the mirror motion was measured to be 1.5 μm across the 150 mm diameter mirror surface over a 400 μm throw.

Commercial piezoelectric actuators (DSM) control the mirror motion. These motors rest perpendicularly to surrounding titanium flexures; elongation of the piezo pushes against these flexures, which subsequently magnify the motion (Fig. 3). We measured the reliable full throw for the piezos to be 400 μm. Crossed flexure universal joints are coupled to each end of the piezoelectric motor. The front universal joint is coupled to an adjustable plate on the front of the motor housing; this allows the user to define the actuator motion relative to the rectangular frame. The back universal joint is connected to the moving mirror stage via an L bracket. The universal joints act to prevent nonparallel motion of the actuator from affecting the mirror motion [15]. A servo-control amplifier controls distance to within 1 μm. The grid–mirror displacement is measured using a capacitive sensor (ADE Technologies) mounted to the bottom of the aluminum frame.

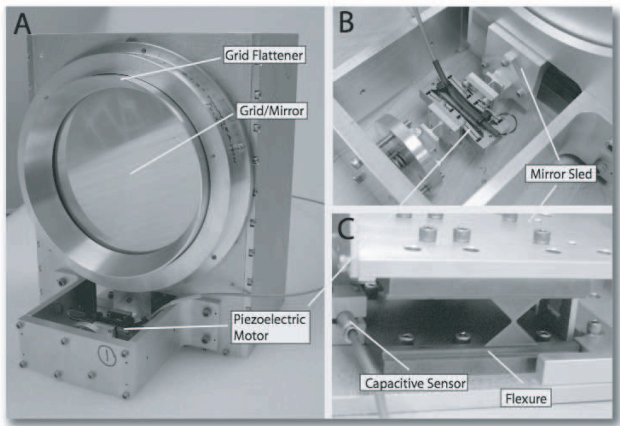

Fig. 3. (Color online) Views of one VPM. A, Front view. Wire grid is held to the front of the aluminum frame by rare earth magnets. Grid flattener increases planarity of wires. Its interior edge is milled to correspond with a 20° incident angle. B, View inside housing for piezoelectric actuator. The motor is surrounded by titanium flexures that magnify the piezo motion. The actuator is connected to two universal joint flexures to couple motion to the mirror and to absorb any twisting motion caused by misalignment. C, Back view under mirror mount, showing double-blade flexure and capacitive sensor. Sensor measures actual mirror–grid separation distance and sends this information to servo controller, completing control loop.

Grid quality was of primary concern in the construction of the VPMs, as error in wire spacing and grid flatness can create grid inefficiencies. We used two 15 cm diameter freestanding grids for the experiment. The grids consist of 25 μm diameter gold-coated wires with a nominal spacing of 63 μm. We measured an actual average grid spacing of 67.5 μm. The grids are specified by the vendor (Millitech) to frequencies up to 1600 GHz (wavelengths greater than 187.5 μm), with a nominal efficiency of 95% at this frequency.

We desire an rms grid flatness that is less than 1% of the operating wavelength. Obtaining straight and parallel wires requires them to be under considerable tension. This tension causes a "potato chip" effect, with the tension on the wires deforming the wire grid frame out of planarity. Because of this effect, we measured the wires in the grids to have an rms flatness of roughly 35 μm, equal to one-tenth of our operating wavelength. To improve grid efficiency, we developed a grid flattener. The flattener has an optically flat end surface which rests against the stretched wire surface [15]. Set screws bring the flattener into contact with the wires just until the wires are deflected, minimizing the stress on the flattener itself. The flattener was able to improve the rms flatness to ~2 μm. Figure 3 shows the flattener; the interior radius was machined at a 20° angle in accordance with the beam incident angle.

The grid assembly is pulled toward the VPM frame with rare-earth magnets embedded in the front plate, while three set screws in the grid assembly push against the front plate, establishing the grid–mirror parallelism. The set screws align with small divets located near the magnets on the front plate to establish repeatable rotational positioning of the wire grid.

Good parallelism between the mirror and grid surfaces is crucial to obtaining accurate phase delays and parallel polarization beams. To set and measure the parallelism, we used a commercial monocular microscope with 200× magnification and mounted it on a linear translation stage with a micrometer, which, in turn, was mounted on a moveable base. This setup is shown in Fig. 4. The aluminum mount for the microscope has mounting holes at two different heights, corresponding to different measurement locations along the edge of the grid.

To begin, we mount the grid to the front of the rectangular frame, aligning the set screws with the corresponding divets on the front surface. Adjustments are made with the set screws to move the grid close to the mirror surface, moving one screw at a time.

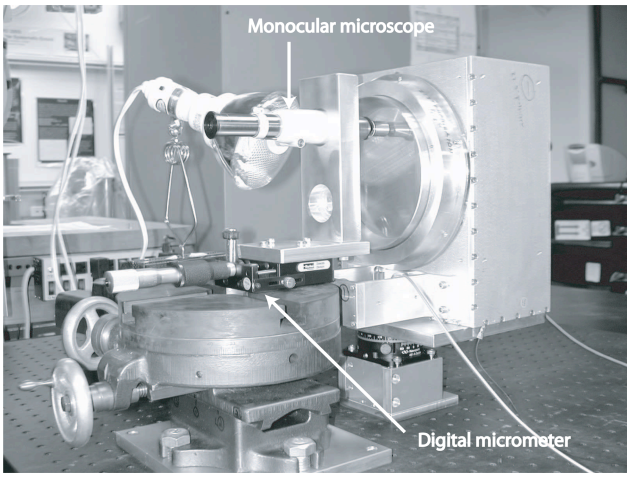

Fig. 4. (Color online) Microscope setup for grid–mirror parallelization measurements. The microscope is mounted on a bracket that is moved toward and away from the grid via a linear translation stage that incorporates a digital micrometer. Measurements are made at three points around the edge of the grid.

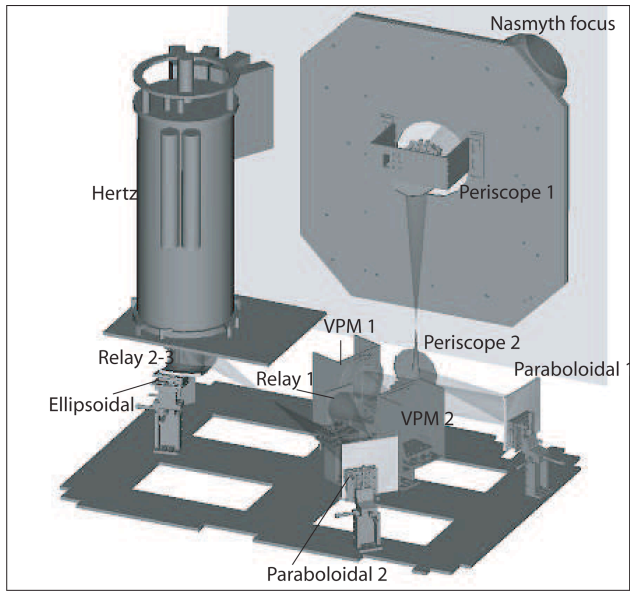

Fig. 5. (Color online) Optics path of Hertz/VPM experiment at SMTO. Optics sit at the Nasmyth focus of telescope. Light is reflected down into the optics plane by two periscope mirrors. Light is collimated with a paraboloidal mirror then passes through the VPMs before being refocused by the second paraboloidal mirror. After refocusing, two relay mirrors send the light to an ellipsoidal mirror, which refocuses the light, this time to match the focal length of Hertz.

A target separation distance is determined, calculated such that the mirror at its closest position is $50\,\mu$m from the grid. Using the microscope, the distance between the grid wires and their reflection is measured and the set screws are adjusted until the separation distance equals the target distance.

We repeat this procedure for each of three points on the wire grid; usually two or three iterations around the circle are needed. The alignment process results in parallelism of roughly $5 \pm 3\,\mu$m.

B. Optical Interface to Telescope

The SMTO is operated by the University of Arizona and is located on Mount Graham, near Safford, Arizona. The site rests at approximately 10,500 feet and has good submillimeter ($\tau_{230\,\mathrm{GHz}} \leq 0.06$) nights roughly 10–15% of the time during the months of December–February with a slightly lower percentage of good submillimeter nights in April. In this and the following two subsections we describe the constructed optics train, the Hertz polarimeter, and the control system for the experiment, respectively.

The Heinrich Hertz Telescope at the SMTO has a 10 m primary and operates between 0.3 and 2 mm wavelengths [16]. The focal ratio at the Nasmyth focus is 13.8. During our observations we chopped the secondary between two sky positions separated by $4'$ in cross elevation at a rate of 3 Hz.

Figure 5 shows the optics path for the experiment. Light from the telescope is incident upon two flat periscope mirrors that bend the light down into the horizontal optics plane. The light is then collimated using an off-axis paraboloidal mirror before reaching the VPMs. VPM 1 has its grid wires rotated 22.5° counterclockwise from the horizontal, while the grid wires for VPM 2 are aligned horizontally. After passing through the modulators, the beam is then refocused using a second off-axis paraboloidal mirror. Next, a series of two additional flat mirrors sends the beam to an ellipsoidal mirror that refocuses the light to match the focal ratio of the Hertz cryostat (4.48). The full experimental setup is shown in Fig. 6. Table 1 lists optics components and their properties. The optics were aligned in a two-step process; the first was a laser alignment of the optics carried out in the laboratory at Arizona. Second, cold-load tests were conducted at SMTO to ensure that the beam was centered on each optical element.

We define the Stokes parameter reference frame for Hertz/VPM by the convention described in Subsection 2.A, with $-Q$ aligned with the Earth's gravitational field. (Thus, $+Q$ is horizontal, $+U$ is 45° counterclockwise (CCW) from horizontal as viewed looking toward the incident beam, etc.) The input polarization is referenced to the input to the polarimeter, which we define to be just before the first paraboloidal mirror (see Fig. 5).

In designing our dual-VPM system, one concern we faced regarding the optics was beam walkoff in the VPMs, the lateral translation between orthogonal components after they have passed through the mirror–grid system. Simple geometry shows that the total walkoff can sum to a significant fraction of the wavelength. We tried to minimize this effect in two ways. The first was to place each VPM as close as possible to a pupil; lateral shifts at a pupil translate only to different incident angles at the focal plane. The angular displacement is directly proportional to the incident angle at the VPMs. Thus, to further minimize walkoff effects we made the incident angle as close to normal as possible. We chose this angle to be 20°,

Table 1. Optics Elements of the Hertz/VPM Experiment and Their Properties

Element	$f/\#$ or focal length	Distance to next optic (mm)	Notes
telescope	13.8	2410.6	
periscope 1	-	777	
periscope 2	-	526	
paraboloidal mirror 1	695 mm	620	off-axis paraboloid
VPM 1	-	300	grid 22.5° CCW from horizontal
VPM 2	-	225	grid horizontal
relay mirror 1	-	537	
paraboloidal mirror 2	695 mm	1161	off-axis paraboloid
relay mirror 2	-	225	
relay mirror 3	-	184	
ellipsoidal mirror	900 mm (input) 360 mm (output)	210	Distance is to Dewar window
Hertz	3.9/3.5	-	pupil lens/detectors

which allowed for sufficient beam clearance through the optics.

C. The Hertz Instrument

Hertz contains two 32-bolometer arrays (6×6 with the corners removed) cooled to 0.3 K via a Helium-3 refrigerator [17]. An analyzer grid splits the incoming signal into two orthogonal linear polarizations and directs each to a detector array. This dual-polarization observing strategy results in a $\sqrt{2}$ increase in the signal-to-noise ratio over single-polarization systems and also aids in removing sky noise, which is correlated between arrays [13]. The polarimeter operates at 350 μm with a relative bandwidth of $(\Delta\lambda)/\lambda = 10\%$. Hertz contains cold reimaging optics using antireflection-coated quartz lenses.

Hertz incorporates a quartz HWP located at a cold pupil stop. Although we did not require this for polarization measurements carried out with the dual-VPM polarimeter, we used it for two purposes: first, by using the Hertz instrument in its original HWP-polarimeter mode, we were able to measure the linear polarization state at the output of the VPMs, providing a diagnostic of the dual-VPM modulator by itself. Second, as mentioned in Subsection 2.C, polarization observations with Hertz/VPM require that the time-reversed polarized light beams from the R and T detector arrays reach VPM 2 with polarization angles rotated by $\pm 45°$ with respect to the grid wires of VPM 2 (e.g., see Fig. 2). It was convenient to achieve this condition by rotating the HWP in Hertz rather than having to rotate the entire Dewar.

We thus needed to determine the HWP angle that satisfied this criterion. At the SMTO, we accomplished this by placing a polarizing grid with horizontal wires in the optics train, directly after VPM 2. We then rotated the HWP until the signals were approximately equal in the R and T arrays. This angle was determined to correspond to an encoder reading of 96° (relative to an arbitrary offset). We collected data at both 96° and the equivalent angle of 51° (which switches only the sign convention of the measured Stokes parameter, as shown in Subsection 2.C).

D. Control System

The control system is outlined in Fig. 7. The main control computer sends commands to the other computers through a user-operated GUI. The main control computer communicates via TCP/IP with three computers: the telescope-control computer, which controls the telescope motion and positioning; the data-acquisition computer, which records bolometer output to file along with header information, displays data onscreen, and controls the chopping secondary mirror; and the Ethernet Data Acquisition System (EDAS) that operates the modulators (HWP and VPMs).

The data-acquisition computer receives, stores and displays data sent from the Hertz detector. Signals originate in Hertz as bolometer voltages that are amplified and then converted to a digital signal via an A/D converter. The data acquisition computer incorporates a custom-built data signal processor (DSP)

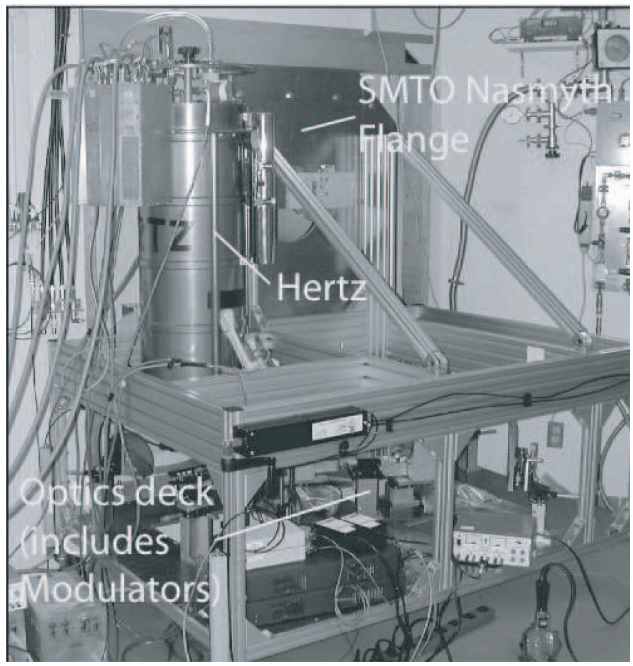

Fig. 6. Photo of the Hertz/dual-VPM experiment at the SMTO. The optics sit at the Nasmyth focus; optics bench mounts to wall via a large flange.

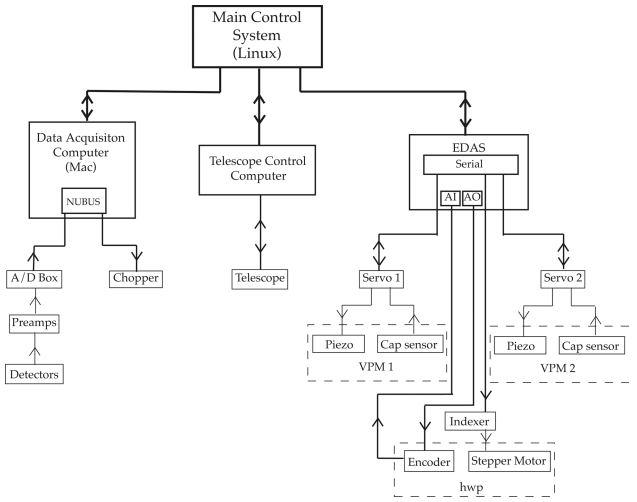

Fig. 7. Diagram of control electronics. Lines signify paths of communication between components; arrows signify direction. Main control computer communicates with three computers via TCP/IP connections. The data-acquisition computer computes demodulated signals from detectors, synchronized by a chopping frequency sent to the secondary mirror. Telescope-control computer handles telescope motion and positioning. EDAS controls both the VPMs and the Hertz HWP.

card. The computer records only the chopper-demodulated (i.e., on-source—off-source) signals. The DSP card performs the demodulation of the incoming data stream in synchronization with the chopper reference signal that it generates and sends to the secondary mirror controller. After demodulation, the data-acquisition computer saves the demodulated data for each pixel to disk.

The EDAS (Intelligent Instruments) is a modular system computer that allows remote operation via an internet connection. Its use of flash memory eliminates the risk of hard drive failure. Three modules are connected to the EDAS main CPU and power modules: a serial port module, an analog-output (AO) module and an analog-input (AI) module.

To move the VPM mirrors, a target position is sent by the main control computer to the EDAS, which sends that command (via binary serial communications) to the servo controller. The servo sends the actual position recorded by the capacitive sensor back to the EDAS (via binary serial) which relays it to the main control computer (via TCP/IP). To rotate the HWP, the EDAS sends serial commands to a stepper motor indexer, which controls the HWP motor. The EDAS measures the HWP position by first applying an output voltage across a HWP encoder via the AO. The custom-built HWP encoder consists of a cryogenic rotary variable resistor mounted to the HWP. The output voltage across the resistor is read by the AI module and is converted to a HWP angle via a simple linear equation determined by previous measurements.

E. Laboratory Test Setup

Next we describe the setup used to carry out testing of the Hertz/VPM polarimeter at Northwestern University. We simulated the telescope signal using a commercial blackbody source placed behind a rotating optical chopper. The blackbody was placed near the focus of the first paraboloidal mirror. To facilitate the mounting and alignment of the blackbody, we removed the two periscope mirrors, replacing them with a flat mirror that keeps the beam in the horizontal optics plane. A polarizing grid (the "calibration grid") was placed between the blackbody and the chopper as needed. The calibration grid was mounted on a rotating support, allowing us to vary the polarization state of the source. We rotated the grid to different angles corresponding to $\pm Q$ and $\pm U$ polarization states.

Some difficulty arose due to extraneous signals caused by the bolometer array viewing an image of itself reflected by the aluminum aperture plate of the blackbody. We were able to eliminate this effect by first rotating the blackbody, grid, and chopper planes slightly away from orthogonality to the beam and then placing a new aperture, drilled from a piece of absorber, in front of the blackbody/grid/chopper system. The optics alignment achieved at Northwestern was not as accurate as that for the SMTO tests. A careful laser alignment of the mirrors was carried out, but no cold-load alignment was done. This may, in part, explain the measured efficiency of the system, as we discuss below.

As described above (Subsection 3.C), at SMTO we used an empirical procedure to determine the fixed HWP angle to be used for polarization measurements using dual-VPM modulators. Because this procedure was carried out before the relative gains f (Subsection 2.C) were determined, it was subject to significant uncertainties. Accordingly, for our laboratory measurements, we used a more accurate method. We rotated the calibration grid wires to an angle 45° CCW from horizontal, or $-U$ input polarization. We collected HWP files (each modulator file consists of one cycle, as defined in Subsection 2.C) with VPM 2 set to a full-wave delay and with the VPM 1 grid removed. We then examined a plot of the polarization signal as a function of HWP angle. The location of the first peak equals the correct HWP angle. We measured this angle to be 80°, a difference of 16° from the previous setting (96°).

During laboratory testing in 2007, we collected many VPM files with the HWP set to the correct angle of 80°. Because of an inadvertent error, we also collected laboratory VPM files at a HWP angle of 68°. In Subsection 4.B we will discuss how erroneous HWP angle settings affect our measurements.

4. Results

To fully characterize the Hertz/VPM polarimeter, we took HWP and VPM files with different input sources (planets or blackbody source), both with and without a polarizing grid (the calibration grid) placed in front of VPM 1. Data taken without the VPM polarizing grids were used to obtain photometry maps and instrumental polarization measurements. Data taken with the calibration grid installed were used to characterize

VPM performance and determine system polarization efficiency. We also confirmed, via observations of multipeaked galactic dust clouds, that the beam size of Hertz is close to 20″. This is consistent with our expectations, since Hertz achieved ∼20″ resolution when used at CSO together with a set of relay optics that gave a plate scale at the Hertz input similar to that given by our SMTO optical design [18].

We present SMTO data collected only on the last night of the run (April 24), as it was the only night of the run with low atmospheric opacity ($\tau_{230\,\mathrm{GHz}} \leq 0.06$) and stable observing conditions. Data taken in the laboratory were collected over a two-week period in October 2007.

A. Observed Asymmetry in the VPM Interferograms

At the SMTO, we observed Saturn through a polarizing grid mounted at the input to the polarimeter (Subsection 3.B) with wires horizontal with respect to the optics plane. We took HWP files with the VPMs set to various combinations of grid–mirror separation distances. The data were fit using a two-VPM transfer function model [11]. This model allowed us to fit for the source polarization, small fixed offsets in the grid–mirror separation of each VPM, and rotational errors in the alignment of the VPM grids. Though the data exhibited the same qualitative features as the model, the measured phase delays of the VPMs did not match the delays one expects given the geometry, wavelength, and reported grid–mirror separation.

We isolated this effect in the laboratory by studying the polarization properties of a single VPM. Using the laboratory setup described above, we removed the grid from the front of VPM 1 and sent polarized light oriented −45° with respect to the horizontal axis ($-U$) directly into VPM 2, whose grid axis is aligned horizontal to the optics plane. We then stepped the grid–mirror separation distance from 50 to 450 μm, roughly two full wavelength cycles of polarization modulation, acquiring a HWP file at each position.

For ideal grid performance (i.e., perfect reflection of polarized light orientated parallel to the grid, perfect transmission of orthogonal polarization) and monochromatic radiation, we expect a unity–amplitude sine modulation of u with extrema located at the theoretical spacings (for $\lambda = 350\,\mu$m) of $(n + 1/2)^{*}186\,\mu$m (VPM "on") and $n^{*}186\,\mu$m (VPM "off"), as we showed earlier in Subsection 2.B. Figure 8 plots normalized Stokes u versus grid–mirror separation distance for VPM 2; each point plotted represents a HWP file taken at one VPM setting. The solid curve represents the theoretical performance of an ideal VPM, but taking into account both the lower overall amplitude and the decoherence due to the finite bandwidth of the system (see Subsection 3.C). For illustrative purposes, we applied an arbitrary offset to align the curve with the first valley of the laboratory data. Note that the data points, unlike the solid curve, show an asymmetry between the ascending and descending portions of the curve; namely, the peak–valley separation distances differ significantly from the predicted values for ideal grids, as calculated in Subsection 2.B. We also observe an amplitude well below unity; a discussion of possible causes for this effect is deferred until Subsection 4.B.

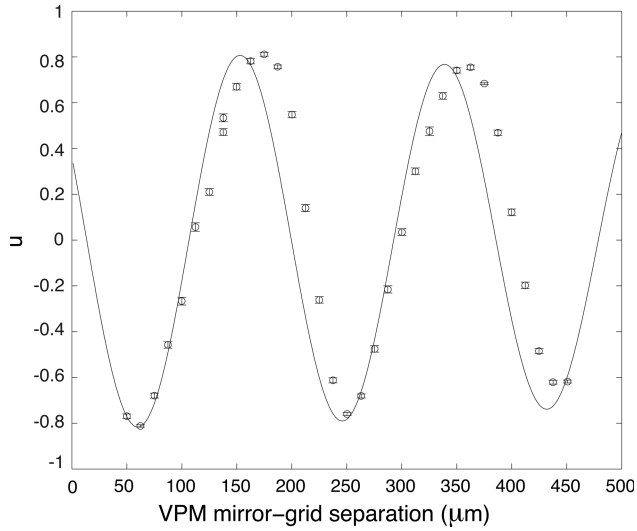

Fig. 8. Interferogram plotting normalized Stokes parameter u versus mirror–grid separation for VPM 2. Input light is assumed to be 100% polarized at an angle of −45° with respect to the $+x$ axis (relative to VPM 2). The solid curve is the signal expected for a geometric phase delay with a 10% bandwidth decoherence. This idealized curve has been modified to match the amplitude and phase of the first peak of the observed data. The data do not match this simple geometrically motivated model; there is an asymmetry in the observed data, with the peak–valley separation distances being significantly different from 93 μm, the predicted value for ideal grids. A more detailed model that includes the phase response of the grid is required to reproduce the observed instrumental performance.

Models exist in the literature for wire grid performance. Using one such model [19] we were able to qualitatively reproduce the aforementioned asymmetry observed in our experimental results for the normalized Stokes u parameter as a function of the grid–mirror separation. We ran a simulation of the corresponding theoretical response of our VPM. The model used the wire radius a and spacing d of our experiment and conductivity values σ that corresponded to aluminum-coated glass mirrors and gold-plated wires (see Subsection 3.A). These results are shown in Fig. 9. The dashed curve represents the interferogram for an idealized VPM, which is a pure sinusoid. The solid curve shows the simulated plot of Stokes u versus the grid–mirror separation distance for the model VPM. The model is calculated for a very narrow bandwidth; thus, we can ignore the spike at the maximum, which is a feature of the low bandwidth. This feature would be washed out for Hertz/VPM.

Similar to the laboratory data, the model shows an asymmetry in the interferogram. The difference between the ideal and model curves is a function of the grid parameters a and d and the operating wavelength λ. Increasing the wavelength by a factor of

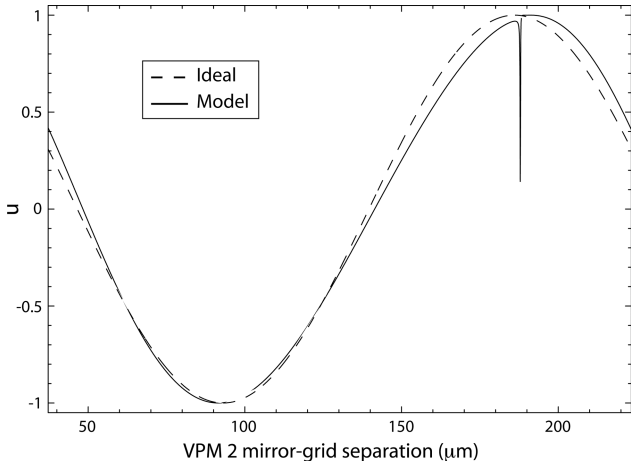

Fig. 9. VPM interferogram obtained using a model that treats wire grid performance [19]. The solid curve shows the model predictions (u versus grid–mirror separation distance) for the case of grid parameters, wavelength, and incident polarization that match our experiment. The model employs a very narrow bandwidth and assumes regular wire spacing. The spike in the solid curve would be expected to be washed out by the large relative bandwidth of Hertz and, indeed, is not observed in Fig. 8. The dashed curve shows the idealized sinusoidal interferogram that would be expected for the case of ideal grid and geometric phase delay. In the long wavelength limit, the model curve approaches the idealized curve.

10 in the model eliminates the observed asymmetry. In our case, $(\lambda/a) = (350/12.5) = 28$. This is somewhat outside of the stated applicability of the model [19] $(\lambda/a > 40)$, which is the likely cause of the remaining discrepancy between the model and observed data.

It is important to note that even though we find that the actual phase delay differs from the geometric prediction, the effect described here does not affect the utility of the VPM. It simply indicates that a more detailed model is required to map the grid–mirror separation into phase. For the purposes of this work, the interferogram in Fig. 8 can be used to "tune" our VPMs. Our interferogram shows that, for the VPM grids used, operating at 350 μm, the peaks and valleys are not at the geometrically motivated values of 186 and 93 μm. It is reasonable to assume that when carrying out VPM cycles (Subsection 2.C) to measure polarization with Hertz/VPM, one will obtain improved performance by applying adjustments to the mirror–grid separation distances so that the full- and half-wave conditions are met. After experimentally determining the proper full- and half-wave delays for VPM 2 to be at 175 and 62.5 μm, respectively (see Fig. 8), we then set the device to a full-wave delay (i.e., turned "off," or 175 μm), and repeated the interferogram measurements for VPM 1, finding extrema at 210 and 75 μm. We collected VPM files using these empirically determined VPM settings as well as other settings related to the theoretical separations, which were later used for comparison.

We note that the proper settings obtained from the interferograms are not the same for each VPM. Although we are not sure of the cause of this difference in settings, we speculate that it may be related to the orientation of the wire grids with respect to the plane of incidence. For VPM 2, the grid wires are parallel to the plane of incidence, while the same is not true for VPM 1.

B. Polarimeter Performance

In Subsection 4.A, we determined key characteristics of the individual VPMs. Now, through analysis of the VPM files collected, we present a series of measurements taken to determine the performance of the complete Hertz/VPM polarimeter.

A key characteristic is the polarization efficiency, defined as the ratio between the input polarization and the polarization actually measured by the polarimeter. For the case of Hertz/VPM, the polarization efficiency is defined as the polarization measured for an assumed 100% polarized input signal. In practice, however, the input polarization is determined by the calibration grid, which does not produce completely polarized light. For our purposes, we consider any efficiency losses of the calibrator grid to be negligible.

As suggested by the interferogram plot in the previous section, there are sources of polarization inefficiency in the experiment. Two main factors that contribute significantly to the measured efficiency of the Hertz/dual-VPM system (see Table 2) are the HWP angle setting used for the VPM files and the VPM settings used. We compare SMTO and labpratory data taken under three different conditions: incorrect HWP and VPM settings (groups 1–3 in Table 2), incorrect HWP setting and correct VPM settings (group 4), and correct HWP and VPM settings (group 5). The determination of the HWP angle settings was discussed previously in Subsections 3.C and 3.E. We note that for group 2, the HWP angle is closer to (80–45 =)35° than to our proper offset angle of 80°; thus, our calculation of Stokes q and u for this group includes an inversion as explained in

Table 2. Modulator Settings and Measured Efficiencies for Datafile Groupings

Group	HWP angle (°)	VPM 1 setting (μm) half wave	Full wave	VPM 2 setting (μm) half-wave	Full wave	Location	Efficiency
1	96	93	186	93	186	SMTO	$54.3\% \pm 2.6\%$
2	51	93	186	93	186	SMTO	$53.8\% \pm 1.2\%$
3	68	100	193	82	175	lab	$47.7\% \pm 15.6\%$
4	68	75	210	62.5	175	lab	$52.3\% \pm 1.8\%$
5	80	75	210	62.5	175	lab	$85.7\% \pm 1.0\%$

Subsection 2.C. Also note that, for group 4, the difference between half- and full-wave delay positions was set to 93 μm, but the positions were offset from the geometric values of 93 and 186 μm.

For SMTO calibration grid data, we collected nine VPM files (four for group 1, five for group 2) of Saturn with a polarizing grid installed before the first paraboloidal mirror. For each of these two groups, files were taken at only one polarizing grid angle (horizontal grid wires, or $-Q$ input polarization). For the laboratory data, group 3 consisted of six files taken at each of four polarizing grid angles ($\pm Q, \pm U$), while groups 4 and 5 included two files taken at each angle. From each VPM file we calculated normalized Stokes q and u by the method outlined in Subsection 2.C. (Again note that for group 2 the calculation includes an inversion; see above.)

Figure 10 shows the nominal input polarization states (denoted by solid circles) together with these q and u measurements. Each plotted measurement represents an average over all files taken at a particular calibration grid angle within one group. The measured angle of polarization was always within 3° of the nominal value (6° in Stokes space). However, the degree of polarization could be as low as 40% for incorrect HWP and/or VPM settings. This suggests that the main effect that results from these incorrect settings is a loss of polarization efficiency. It is important to note that there are variations in the polarization efficiency as one travels around the Stokes plane. For example, q polarization efficiency is higher than u efficiency for groups 3 and 5, but the reverse is true for group 4. This phenomenon is not fully understood; however, it is evident that using the proper modulator settings results in an overall increase in efficiency.

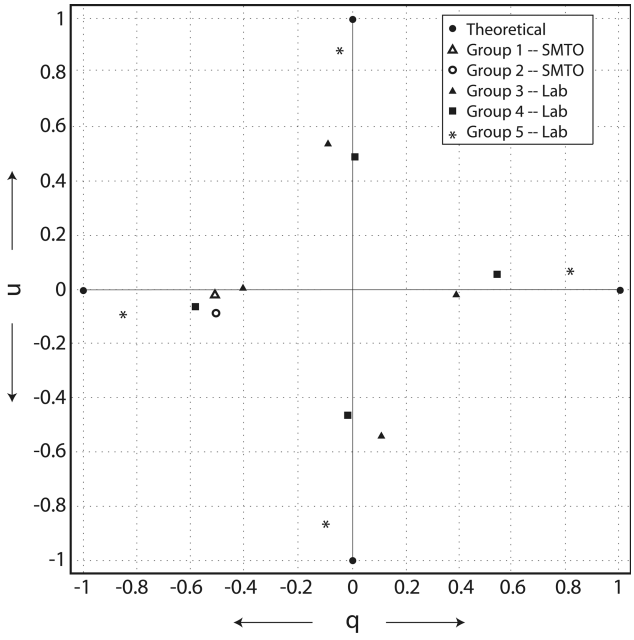

Fig. 10. Polarization measurements made with Hertz/VPM polarimeter. Solid circles on axes represent 100% input polarization. Points plotted represent average values calculated for each group. In qu space, points are rotated away from axes by up to 6°; in real space, polarization angles are within 3° of nominal values. Overall efficiencies increase as HWP and VPMs are moved to their proper settings. For group 2, $u \rightarrow -u$ and $q \rightarrow -q$, as described in Subsections 2.C and 4.B.

We calculated the mean polarization efficiency for each group by averaging over all files in a group, regardless of whether that file was a measure of Q- or U-like polarization. Averages were calculated with equal weighting and are listed in Table 2. The polarization efficiency reached a maximum of roughly 85% for group 5, where the HWP and VPMs are set to their correct positions. Polarization efficiency at the SMTO (groups 1 and 2) was measured to be 54%.

Additional sources of efficiency loss can also be found within Hertz; namely, its HWP and polarizing grids. In the laboratory we collected HWP files taken with the calibration grid in place and with both VPM grids removed. We took files for four polarizing grid angles, corresponding to input polarization of $\pm q$ or $\pm u = -1$. With this configuration, we measured an average efficiency of 93%. Previous measurements for the Hertz polarimeter give an efficiency of 95% [18]; this drop of 2% may be attributable to the quality of the calibration grid, which has not been independently measured.

Even when the VPMs are set to the proper half- and full-wave delays, we still see a maxiumum efficiency of only 85%; for perfect VPM efficiency, we should expect a system efficiency closer to 93%. We do not know the cause of this net dual-VPM efficiency loss; it may be attributable to poor optical alignment in the laboratory (see Subsection 3.E).

VPM files of Jupiter were collected with no calibration grid on the last night of observations at SMTO. The planet is assumed to be unpolarized [20]; hence any detected polarization should be attributed to the instrumental polarization of the full Hertz/VPM system. We collected 15 VPM files taken with the HWP and VPM settings as given for group 1 of the calibration grid files, and 14 files with group 2 settings.

Similar to the data analysis method used for polarized grid files, we calculated the normalized q and u values for each VPM file. Averages were calculated for each group with equal weighting and the q_{ave} and u_{ave} values were combined to give a percent polarization P and angle φ. The results were $0.29 \pm 0.06\%$ and $0.28 \pm 0.1\%$ for groups 1 and 2, respectively. Recall from the previous section that these data were taken with incorrect settings for both the HWP and VPMs; thus, these results should be modified to reflect the lowered system efficiency. Even so, these data suggest that the instrumental polarization of Hertz/VPM is below 1%.

5. Conclusions

The dual-VPM system, which operates in reflection with only small linear translations, is able to simulate the action of a rotating HWP. The inherent properties of the dual-VPM modulator provide numerous benefits: high durability, easy multiwavelength

operation, and sensitivity to circularly polarized light.

Maximization of the dual-VPM system performance requires a full characterization of the performance of the grid–mirror system. The VPM grid properties, in particular wire diameter and spacing, are important contributing factors to whether or not the grid will act ideally for a particular wavelength. If wire grids are to be used at wavelengths shorter than those for which they are optimal, inteferograms can be used to determine proper settings for half- and full-wave phase delays.

Despite these complications, we found that the Hertz/dual-VPM polarimeter has high polarization efficiency ($\sim$85%) and low instrumental polarization ($\leq$1%). Thus, the new device appears to be robust and is a viable option for millimeter/submillimeter/IR astronomy applications, including the numerous experiments currently under development.

We thank Dominic Benford for his support of this work. This material is based upon work supported by the National Aeronautics and Space Administration under grants NNG056K286, NNX07AB85G, NNG-05GG42G and NNX07AI27G, issued through the Science Mission Directorate. M. Krejny was supported by Graduate Student Researchers Program grant NNG05-GL31H. H. Hui was supported by an Undergraduate Student Research Program grant at Goddard Space Flight Center.

References

1. W. A. Hiltner, "Polarization of light from distant stars by interstellar medium," Science **109**, 165 (1949).
2. J. S. Hall, "Observations of the polarized light from stars," Science **109**, 166–167 (1949).
3. S. Chandrasekhar and E. Fermi, "Magnetic fields in spiral arms," Astrophys. J. **118**, 113–115 (1953).
4. A. Lazarian, "Physics of grain alignment," in *Cosmic Evolution and Galaxy Formation: Structure, Interactions, and Feedback*, ASP Conference Series, Vol. 215, J. Franco, L. Terlevich, O. Lopez-Cruz, and I. Aretxaga, eds. (Astronomical Society of the Pacific, 2000), pp. 69–78.
5. W. I. Cudlip, I. Furniss, K. J. King, and R. E. Jennings, "Far infrared polarimetry of W51A and M42," Mon. Not. R. Astron. Soc. **200**, 1169–1173 (1982).
6. R. H. Hildebrand, M. Dragovan, and G. Novak, "Detection of submillimeter polarization in the Orion nebula," Astrophys. J. **284**, L51–L54 (1984).
7. D. T. Chuss, D. J. Benford, C. Walker, S. H. Moseley, G. Novak, J. G. Staguhn, and E. J. Wollack, "A 350 μm array polarimeter using translational modulators," Proc. SPIE **5492**, 1450–1460 (2004).
8. J. D. Jackson, *Classical Electrodynamics*, 3rd ed. (Wiley, 1999).
9. H. Shinnaga, M. Tsuboi, and T. Kasuga, "A millimeter polarimeter for the 45 m telescope at Nobeyama," Publ. Astron. Soc. Jpn. **51**, 175–184 (1999).
10. G. Siringo, E. Kreysa, L. A. Reichertz, and K. M. Menten, "A new polarimeter for (sub)millimeter bolometer arrays," Astron. Astrophys. **422**, 751–760 (2004).
11. D. T. Chuss, E. J. Wollack, S. H. Moseley, and G. Novak, "Interferometric polarization control," Appl. Opt. **45**, 5107–5117 (2006).
12. E. S. Battistelli, M. DePetris, L. Lamagna, R. Maoli, F. Melchiorri, E. Palladino, and G. Savini, "Far infrared polarimeter with very low instrumental polarization," arXiv:astro-ph/0209180v1.
13. R. H. Hildebrand, J. A. Davidson, J. L. Dotson, C. D. Dowell, G. Novak, and J. E. Vaillancourt, "A primer on far-infrared polarimetry," Publ. Astron. Soc. Pac. **112**, 1215–1235 (2000).
14. S. R. Platt, R. H. Hildebrand, R. J. Pernic, J. A. Dotson, and G. Novak, "100 μm Array polarimetry from the kuiper airborne observatory: instrumentation, techniques, and first results," Publ. Astron. Soc. Pac. **103**, 1193–1210 (1991).
15. G. M. Voellmer, D. T. Chuss, M. Jackson, M. Krejny, S. H. Moseley, G. Novak, and E. J. Wollack, "A kinematic flexure-based mechanism for precise parallel motion for the Hertz variable-delay polarization modulator (VPM)," Proc. SPIE **6273**, 114 (2006).
16. J. W. M. Baars, R. N. Martin, J. G. Mangum, J. P. McMullin, and W. L. Peters, "The Heinrich Hertz Telescope and the Submillimeter Telescope Observatory,"Publ. Astron. Soc. Pac. **111**, 627–646 (1999).
17. D. A. Schleuning, C. D. Dowell, R. H. Hildebrand, S. R. Platt, and G. Novak, "Hertz, a submillimeter polarimeter," Publ. Astron. Soc. Pac. **109**, 307–318 (1997).
18. C. D. Dowell, R. H. Hildebrand, D. A. Schleuning, J. E. Vaillancourt, J. L. Dotson, G. Novak, T. Renbarger, and M. Houde, "Submillimeter array polarimetry with Hertz," Astrophys. J. **504**, 588–598 (1998).
19. M. Houde, R. L. Akeson, J. E. Carlstrom, J. W. Lamb, D. A. Schleuning, and D. P. Woody, "Polarizing grids, their assemblies, and beams of radiation," Publ. Astron. Soc. Pac. **113**, 622–638 (2001).
20. D. P. Clemens, B. D. Kane, R. W. Leach, and R. Barvainis, "Millipol, a millimeter/submillimeter wavelength polarimeter—instrument, operation, and calibration," Publ. Astron. Soc. Pac. **102**, 1064–1076 (1990).